Mathematical equations for pressure relief angle of protective seam inclination in outburst coalmine

Zhen Zhang
Henan Polytechnic University
Gaofeng Liu (liugaofeng82@163.com)
Henan Polytechnic University https://orcid.org/0000-0002-9340-9029
Ting Ren
University of Wollongong
Patrick Booth
University of Wollongong
Runsheng Lv
University of Wollongong
Jia Lin
University of Wollongong

Research

Keywords: coal and gas outburst, protective seam mining, protected scope, pressure relief angle, coal seam dip

Posted Date: August 4th, 2020

DOI: https://doi.org/10.21203/rs.3.rs-49991/v1

Abstract

Protective seam mining is one kind of most effective measure to reduce coal and gas outburst risk. The pressure relief angles along inclination (δ_m) are key parameters for evaluating the effect of protective seam mining. However, the numerical relation between δ_m and coal seam dip (a) is defined by discrete data and is difficult to determine δ_m accurately. In this study, the variations of δ_m with respect to seam dips are analyzed to derive analytical equations that can be used to accurately calculate δ_m. The relationship between δ_m and seam dip (a) can be expressed as parabolic or inverted parabolic curves. Mathematical equations for δ_m are derived by curve fitting technique. Furthermore, polynomial equations are determined as the most appropriate for δ_m calculation when the polynomial order is selected as 7, 6, 4 and 5 respectively. These derived equations are computationally solved and verified using actual and field test data of $\delta_{m.}$ with satisfactory consistency and accuracy. The equations are suggested as supplement and improvement for Detailed Rules on Prevention of Coal and Gas Outburst.

1. Introduction

Coal and gas outbursts are one of the greatest natural hazards in underground coalmining, which continue to threaten safety and limit production. Many countries have experienced coal and gas outbursts in underground mining (Aguado and Nicieza, 2007; Black, 2019; Hedlund, 2012; Saleh and Cummings, 2011; Skoczylas et al., 2014; Sobczyk, 2014; Wang et al., 2014). Coal is a major energy resource and plays a critical role in the development of the national economy and society. This situation is expected to remain for a considerable time in China (Feng et al., 2018; Xie et al., 2011; Zhang et al., 2018). However, the main coal-bearing strata in China had undergone complex and multi-stage tectonic movement superposition and evolution, which leads to the formation of widely distributed tectonically deformed coal deposits. The tectonically deformed coal is characterized by low permeability, hard to drain and prone to coal and gas outburst. In-situ stress, gas pressure and gas content typically increase with mining depth in Chinese coal mines, and as a result, the risk of coal and gas outburst also increases. Gas related hazards are still the primary risks affecting coal mine safety (Chen et al., 2019a; Chen et al., 2019b; Han et al., 2012; He et al., 2010; Liang, 2018; Wang et al., 2018; Wang et al., 2012; Wu et al., 2011; Xie et al., 2015; Yin et al., 2017; Zhang et al., 2019).

Two outburst prevention measures, protective seam mining and pre-drainage of coal seam gas, are typically implemented before mining in outburst-prone coal seams (Chen et al., 2019b; Safety, 2019; Skoczylas et al., 2014). Research and engineering practices show that protective coal seam mining is one of the most effective measures to prevent coal and gas outburst. Applications of protective seam mining have clearly demonstrated to significantly reduce risks associated with coal and gas outburst in coal mines in China (Jin et al., 2016; Li et al., 2014; Liu and Cheng, 2015; Wang et al., 2013b; Yang et al., 2011). Furthermore, protective seam mining and pressure-relief gas drainage were applied in low permeability and outburst-prone coal seams to achieve co-extraction of coal and seam gas (Shang et al., 2019; Tu and Cheng, 2019; Wang, 2016; Wang et al., 2013a; Yuan, 2016; Zhang et al., 2020).

Detailed Rules on Prevention of Coal and Gas Outburst (*DRPCGO*), which is promulgated by China's State Administration of Work Safety (Safety, 2019), specifies that protective seam mining must be given priority in outburst-prone coal seams when the relevant conditions are met. *DRPCGO* is currently the most authoritative management and technical legal document on the prevention of coal and gas outburst in China. Moreover,

protective seam mining has also been introduced to prevent rock burst in underground coalmine as a China National Standard (GB/T 25217.12–2019)(State administration of market ragulation, 2019; Xu et al., 2019).

The pressure relief angle along inclination is one of key parameters defining the effective protected area. Two methods can be employed to determine the protected zone along an inclination, including field-testing and data reference according to Appendix *E* in *DRPCGO* (Safety, 2019). Generally, adopting field-testing to determine the protection range along an inclination requires drilling boreholes for measurement of parameters including gas pressure, gas content and maximum expansion deformation rate of the protected seam, etc.(Cao et al., 2018; Jin et al., 2016; Li et al., 2014; Liu et al., 2017; Xue and Yuan, 2017; Yuan and Xue, 2014). *DRPCGO* also emphasizes that historical data reference can be applied to estimate the effective protected zone when there is no field-testing data or the first time to exploit the protective seam in a coal mine (Safety, 2019). Several studies reported the protected zone along inclination can be evaluated by using numerical stimulation to investigate the characteristic of deformation of coal seam, pressure relief rule and gas flow etc.(Jia et al., 2013; Liu et al., 2013; Wang et al., 2010; Zhang et al., 2016). The method of numerical stimulation presents a potential approach for estimating the effective protected zone. However, it is not be applied widely as a criterion because it has not yet established a set of general simulation method and parameters.

Issues will typically be encountered in estimating the protected zone along inclination by using data reference according to Appendix *E* in *DRPCGO*. As the relationship between pressure relief angles and coal seam dip is defined by discrete data, as shown in Table 1, where it is difficult to determinate the precise values of pressure relief angles directly. To solve this issue, this study analyzed the variation of pressure relief angles with seam dips to establish mathematical models for pressure relief angles calculation for protective seam mining. The models have been demonstrated to be of high precision and ease of use for engineering application.

2. Methodology

2.1. Principle of eliminating outburst with protective seam mining

The protective seam refers to the coal seam or strata that is mined out first to eliminate or weaken the outburst hazard of the adjacent coal seams. Figure 1 illustrates that the upper and lower seams undergo deformation after mining of the protective seam, and due to this influence, the in-situ stress decreases and the permeability is typically enhanced. Additionally, a large volume of gas is liberated and pre-drained, decreasing the gas pressure and gas content in adjacent coal seams so that the outburst risk of the protected seam is reduced (Wang et al., 2017b; Wang et al., 2013b; Xie and Xu, 2017; Yang et al., 2011; Yin et al., 2015; Yuan, 2016).

For dipping seams, as shown in Fig. 2, the boundary of the pressure relief zone is elliptical after the protective seam is mined, and the minor axis is approximately equal to the width of the mined-out area. Moreover, the length of two half major axes are not equal, and the length in the roof is longer than that in the floor. Because the upper strata will cave after mining, and the influence range in the roof is also larger than that in the floor (Cheng, 2010; Yu, 1986).

2.2. Definition of pressure relief angles along seam inclination

Based on Appendix *E* in *DRPCGO*, as shown in Fig. 3, A represents the protective seam, and B_1 and B_2 represent the protected seams. *A* is the lower protective seam relative to B_1 and is the upper protective seam relative to B_2. The pressure relief range is determined by the seam dip *a*, the pressure relief angles δ_1, δ_2 for the upper seam B_1, and δ_3, and δ_4 for the lower seam B_2. *C* is the protective boundary.

Based on underground coal mining theory, the caving zone of the inclined coal seam is quite different from that of the horizontal coal seam in long wall mining. As shown in Figs. 4–5, after mining of a flat coal seam, the caving zone will typically exhibit a symmetrical structure. For mining of an inclined coal seam, the caving zone will form an asymmetrical shell structure. When the dip angle of coal seam α exceeds 70°, the shell structure will not exist, and the caving zone will be more complex (LIU and YANG, 2013; Yongqi, 2004). Therefore, the pressure relief angles are related to coal seam dip and the mechanical properties of coal and adjacent strata, but primarily depend on seam dips (Safety, 2019; Yu, 1986).

According to Appendix *D* in *DRPCGO*, the protection zone of the protective seam along the inclination can be delineated according to the pressure relief angle (δ_m, m = 1, 2, 3 and 4), as shown in Fig. 3. If the pressure relief angles cannot be measured, historical data can be referred to Table 1, which was first established by experimental simulation from the Institute of Mining Survey in the former Soviet Union (Yu, 1986).

As shown in Table 1, the relationship between the pressure relief angles and the coal seam dip is defined by discontinuous discrete data sets. This makes it difficult to infer values of relief angles for coal seam dips fall between the discrete datasets. Therefore, a mathematical function for the relationship between pressure relief angle and coal seam dip is required to solve this problem.

Table 1
Relationship between coal seam dip and pressure relief angle (Safety, 2019)

Coal Seam Dip (a / °)	Pressure relief angles (δ_m / °)			
	δ_1	δ_2	δ_3	δ_4
0	80	80	75	75
10	77	83	75	75
20	73	87	75	75
30	69	90	77	70
40	65	90	80	70
50	70	90	80	70
60	72	90	80	70
70	72	90	80	72
80	73	90	78	75
90	75	80	75	80

2.3. Modelling principle

As shown in Table 1, each coal seam dip value (set to x) has a relief angle value (set to y) corresponding to it, which can be represented by a data array (x_i, y_i) (i = 1,2…n). For the convenience of calculation and use, an analytical equation $y = f(x, c)$ is needed to reflect the numerical relationship between the quantity x and y. $y = f(x, c)$ is called the fitting model, and c= (c_1, c_2, •••, c_n) is the parameter to be solved in the equation.

For solving the functional relationship between coordinates represented by discrete point arrays, interpolation and curve fitting are one of the most common data processing methods. The difference is that the interpolation requires all data points to be on the curve, while the curve fitting just requires the curve to reflect the varying trend of the data, and all data points being on the curve are not necessary.

Interpolation methods rely more on measured interpolation reference data points. When there are only a few data points, a simple polynomial equation may be established. However, for the case of more data points, it is not easy to use the interpolation method. Typically, in this scenario, the order of the polynomial needs to be high, the calculation is complex, and the result is not reliable. In contrast, piecewise interpolation may be applied by constructing a linear or polynomial equation in each interval (Tibshirani, 2014). However, it is still not the best selection with complex mathematical equations limiting its application. As a primary estimation, there would not be less 2 or 3 intervals if using the piecewise interpolation for any δ_m, it is estimated that every model includes 2 or 3 equations, by which the pressure relief angles can be estimated, nevertheless, the complex expression of a model with several equations is an obvious shortcoming. It is better to consider curve fitting that can obtain a certain functional relationship, which is convenient for calculation and application (Guest, 2012). Curve fitting was applied as the tool to establish the mathematical function in this research.

The general steps to establish the mathematical model by curve fitting are as follows.

1. Draw the scatter plot;
2. Choose a suitable curve type based on the distribution of scatter points;
3. Fit the equation based on the principle of least squares;
4. Solve the function expression about the original variables *x* and *y*;
5. Model error analysis and accuracy testing.

3. Results And Discussion

3.1. Selection of curve fitting type

According to the reference data in Table 1, we can draw scatter plots of the pressure relief angles with the coal seam dip by Origin 8 software, as shown in Fig. 6.

As shown in Fig. 6, δ_1 and δ_4 decrease first, then remain stable and finally increase with □, and the curves are like the inverted parabolic. By contrast, δ_2 and δ_3 increase first, then remain stable and lately decrease with □, and the curves are like the parabolic. As widely accepted, it is suitable for parabolic or inverted parabolic to use the polynomial curve fitting(Guest, 2012). Therefore, the polynomial fitting was severed as the tool for modelling in the research.

3.2. Parameter solving

For *n* sets of measured data (δ_{mi}, a_i), the characteristic curve δ_m - *a* can be approximately expressed by *n*-1 orders polynomial of a_i by curve fitting (Deboeverie et al., 2010). The polynomial function can be expressed:

$$\delta_{mn} = c_{m1} + c_{m2} a_m + c_{m3} a_m^2 + \ldots + c_{mn} a_m^{n-1} \quad (1)$$

Where, δ_{mn} is the pressure relief angle, m = 1, 2, 3 and 4; c_{m1}, c_{m2}, c_{m3}, ••, c_{mn} are the fitting parameters; n is the total quantity of samples.

Its matrix expression is:

$$\begin{bmatrix} \delta_{m1} \\ \delta_{m2} \\ \vdots \\ \delta_{mn} \end{bmatrix} = \begin{bmatrix} 1\ \alpha_{m1}\ \alpha_{m1}^2 \cdots \alpha_{m1}^{n-1} \\ 1\ \alpha_{m2}\ \alpha_{m2}^2 \cdots \alpha_{m2}^{n-1} \\ \vdots\ \vdots\ \vdots\ \vdots\ \vdots \\ 1\ \alpha_{mn}\ \alpha_{mn}^2 \cdots \alpha_{mn}^{n-1} \end{bmatrix} \times \begin{bmatrix} c_{m1} \\ c_{m2} \\ \vdots \\ c_{mn} \end{bmatrix}$$

2

The curve fitting parameters (c_{m1}, c_{m2}, c_{m3}, ••, c_{mn}) can be easily solved by using the Origin 9.0 software based on the principle of least squares

(Seifert, 2014).

3.3. Polynomial fitting equations

As shown in Table1, there are ten data arrays for each δ_m. Based on the polynomial fitting theory, eight polynomial equations, of orders from 2 to 9, can be derived by polynomial fitting for δ_1, δ_2, δ_3 and δ_4, respectively. In principle, if the order is too low, the fitting accuracy will be too low to meet the requirement. However, if the order is too high, the fitting curve will be locally oscillatory known as “Runge” phenomenon, which will result in low precision (Deboeverie et al., 2010; Fornberg and Zuev, 2007). Therefore, the rational selection of polynomial order is crucial for equation.

In general, the following principles and steps can be employed to determine the appropriate order polynomial equations.

Step 1: a general principle can be used to evaluate the accuracy of fitting result by Determination Coefficient (R^2) and Residual Sum of Squares (*RSS*). The smaller the *RSS* is and the closer R^2 is to 1, the better is the fitting result. However, this principle is not applicable for higher order equation which will usually incur Runge’s phenomenon (Boyd, 2010; Deboeverie et al.,2010).

The expressions of R^2 and *RSS* are as follows:

$$R^2 = \left(\frac{\sum [(\delta_{mi} - \bar{\delta}_m)(a_i - \bar{a})]}{\sqrt{\sum (\delta_{mi} - \bar{\delta}_m)^2} \times \sqrt{\sum (a_i - \bar{a})^2}} \right)^2$$

3

$$RSS = \sum_{i=1}^{n} \left(\delta_{mi} - \hat{\delta}_{mi} \right)^2$$

Where, δ_{mi} is the actual value of pressure relief angle, m=1, 2, 3 and 4; i is the number of samples, i = 1, 2, 3, …, n; is the mean value of δ_m; a_i is the value of coal seam dip; is the mean value of coal seam dip; is the predicted value of pressure relief angle.

Using Origin 9.0 software, the polynomial equations from order 2 to order 8 and the *RSS* and R^2 of four pressure relief angles can be determined respectively, as shown in Table 2.

Based on the data in Table 2, the curves of *RSS* and R^2 with the polynomial order for δ_m are plotted in Fig.7.

Table 2 Result of *RSS* and R^2 on polynomial fitting for δ_m

Order	δ_1		δ_2		δ_3		δ_4	
	RSS	R^2	*RSS*	R^2	*RSS*	R^2	*RSS*	R^2
2	33.23	0.73	25.58	0.80	14.06	0.64	18.50	0.77
3	24.61	0.77	20.78	0.81	2.86	0.92	6.94	0.90
4	19.40	0.78	12.38	0.87	1.99	0.93	5.27	0.91
5	9.48	0.87	0.81	0.99	1.97	0.91	4.34	0.90
6	8.02	0.85	0.55	0.99	1.30	0.92	4.30	0.87
7	3.84	0.89	0.38	0.99	0.39	0.97	2.74	0.88
8	2.86	0.84	0.04	1.00	0.20	0.96	0.22	0.98
9	/	/	/	/	/	/	/	/

As shown in Table 2 and Fig.7, *RSSs* decrease dramatically with the order increasing for δ_m, but when the order reaches or exceeds a certain value that is 5 for δ_1, δ_2, and 3 for δ_3, δ_4, this decreasing trend becomes gentle. On the contrary, R^2 generally increases with the order, but it fluctuates locally. Besides, the value of R^2 for δ_1, δ_2, δ_3, and δ_4 reaches the maximum to 0.89, 1.00, 0.97 and 0.98 at order 7, 8, 7 and 8, respectively.

Step 2: the high orders with Runge's phenomenon need to be eliminated. In this study, it was found that the fitting curves for δ_1, δ_2, δ_3 and δ_4 all appeared "Runge" phenomenon when the order reached as 8, 9, 7 and 8, respectively. The results can be seen in Fig.8.

According to the above analysis, the low orders (from 2 to 4 for δ_1 and δ_2; 2 for δ_3 and δ_4) and the high orders (from 8 to 9 for δ_1 and δ_4, 9 for δ_2, and from 7 to 9 for δ_3, respectively) can be eliminated. Based on step1 and step

2, the following orders (from 5 to 7 for δ_1, from 5 to 8 for δ_2, from 3 to 6 for δ_3, and from 3 to 7 for δ_4, respectively) can be further selected by step 3 and step 4.

Step 3: in some conditions, *RSS* of an equation may be rather small, but it only represents the overall error of the equation. The orders need to be eliminated if the predicted values seriously deviate from the actual values in local points because it is unable to meet the practical precision requirement (Deboeverie et al., 2010; Guest, 2012; Karakus, 2013). To solve this problem, the maximum absolute error (*MAE*) was compared between different polynomial order equations, and the minimum value of *MAE* is used to determine a high-precision equation. As shown in Fig.9, the minimum value of *MAE* can be derived for δ_1, δ_2, δ_3 and δ_4 when the orders are 7, 8, 5 and 6, respectively. Based on this analysis, the equations with the highest accuracy can be determined.

Step 4: is to evaluate the computational complexity of derived equations. It is more convenient to calculate the value of δ_m using a lower order equation that has fewer parameters and a simpler expression. A lower order model can be given priority provided the model precision is satisfied (Deboeverie et al., 2010; Karakus, 2013; O'Hagan, 1978) and the most reasonable equations for δ_1, δ_2, δ_3 and δ_4 can be determined when the model orders are selected as 7, 6, 4 and 5 by Fig.9, respectively, as shown in Table 3.

Table 3 Results of the polynomial fitting equations for δ_1, δ_2, δ_3 and δ_4

δ_m/°	Order	Polynomial fitting equations
δ_1	7	δ_1=80.0262-1.4047a+0.22481a^2-0.01611a^3+5.22676E-04a^4-8.42467E-06a^5+6.63072E-08a^6 -2.03665E-10a^7
δ_2	6	δ_2 =79.98986+0.14557a+0.02205a^2-6.36094E-04a^3+4.8344E-07a^4+1.21955E-07a^5-9.02778E-10a^6
δ_3	4	δ_3 =75.1049-0.17084a + 0.01321a^2-1.91336E-4a^3+7.28438E-7a^4
δ_4	5	δ_4 =74.87972+0.3403a-0.03398a^2+8.53671E-04a^3-8.79371E-06a^4+3.46154E-08a^5

3.4. Equation testing and evaluation

The proposed polynomial equations were tested using error analysis, fitting curve comparison and case verification to evaluate the accuracy and reliability.

3.4.1. Accuracy analysis

Based on the data in Table 1, the formulas in Table 3 are used to calculate the predicted value of δ_m, and the absolute error and relative error for δ_m are also calculated and summarized in Table 4. Table 4 shows the

maximum value, minimum value and mean of the absolute error of the equations for δ_m are 1.56°, 0.01° and 0.47°, respectively. The maximum value, minimum value and mean of the relative error are 2.08%, 0.01% and 0.63%, respectively. For the purpose of comparison, the actual value and the predicted value of δ_m were plotted in Fig.10. It intuitively shows the curves of predicted value are consistent with the actual results, and verifies the validity of the equations for δ_1, δ_2, δ_3 and δ_4.

Table 4 Results of error analysis on polynomial fitting equations for δ_1, δ_2, δ_3 and δ_4

a /°	δ_m/°	Actual value /°	Predicted value /°	Absolute error /°	Relative error /%	δ_m /°	Actual value /°	Predicted value /°	Absolute error /°	Relative error /%
0.00	δ_1	80.00	80.03	0.03	0.03	δ_2	80.00	79.99	0.01	0.01
10.00	δ_1	77.00	76.80	0.20	0.26	δ_2	83.00	83.03	0.03	0.04
20.00	δ_1	73.00	73.63	0.63	0.86	δ_2	87.00	87.04	0.04	0.05
30.00	δ_1	69.00	67.78	1.22	1.77	δ_2	90.00	89.72	0.28	0.31
40.00	δ_1	65.00	66.08	1.08	1.67	δ_2	90.00	90.41	0.41	0.46
50.00	δ_1	70.00	69.02	0.98	1.40	δ_2	90.00	89.91	0.09	0.10
60.00	δ_1	72.00	71.65	0.35	0.48	δ_2	90.00	89.69	0.31	0.35
70.00	δ_1	72.00	71.35	0.65	0.90	δ_2	90.00	90.41	0.41	0.46
80.00	δ_1	73.00	71.83	1.17	1.60	δ_2	90.00	89.84	0.16	0.18
90.00	δ_1	75.00	73.44	1.56	2.08	δ_2	80.00	80.06	0.06	0.08
0.00	δ_3	75.00	75.10	0.10	0.14	δ_4	75.00	74.88	0.12	0.16
10.00	δ_3	75.00	74.53	0.47	0.62	δ_4	75.00	75.65	0.65	0.87
20.00	δ_3	75.00	75.56	0.56	0.74	δ_4	75.00	73.63	1.37	1.83
30.00	δ_3	77.00	77.29	0.29	0.38	δ_4	70.00	71.27	1.27	1.82
40.00	δ_3	80.00	79.03	0.97	1.22	δ_4	70.00	69.78	0.22	0.31
50.00	δ_3	80.00	80.22	0.22	0.28	δ_4	70.00	69.48	0.52	0.74
60.00	δ_3	80.00	80.52	0.52	0.65	δ_4	70.00	70.24	0.24	0.34
70.00	δ_3	80.00	79.74	0.26	0.33	δ_4	72.00	71.88	0.12	0.17
80.00	δ_3	78.00	77.85	0.15	0.19	δ_4	75.00	74.62	0.38	0.51
90.00	δ_3	75.00	75.04	0.04	0.05	δ_4	80.00	79.45	0.55	0.69

3.4.2. Case verification

A case verification was conducted to further evaluate the precision and reliability of the derived equation. The pressure relief angles δ_m were calculated for different cases of coal seam dip, and compared with field results reported by previous studies, as shown in Table 5.

Table 5 Results of the case verification

CaseNo.	Type	Dip/°	δ_m/°	Field value /°	Predicted value /°	Absolute error /°	Relative error /%	Coal mine	Reference
1	Lower	23	δ_1	72.80	71.80	1.00	1.38	Zhu Xian Zhuang	(Jin et al., 2016)
2			δ_2	87.20	88.05	0.85	0.97		
3	Lower	30	δ_1	69.00	67.78	1.22	1.77	Da He	(Cao et al., 2018)
4			δ_2	90.00	89.72	0.28	0.31		
5	Upper	13.5	δ_3	80.00	74.76	5.24	6.55	Xie Qiao	(S, 2019)
6			δ_4	78.00	75.10	2.90	3.71		
7	Lower	3	δ_1	79.00	77.44	1.56	1.97	Si He	(Xiong, 2014)
8			δ_2	81.60	80.61	0.99	1.22		
9	Lower	86	δ_1	73.00	73.58	0.58	0.80	Wu Dong	(Rong H, 2019)
10			δ_2	90.00	85.92	4.08	4.53		
11	Lower	13	δ_1	75.00	76.47	1.47	1.96	Jiu Long	(Zhao Z, 2016)
12			δ_2	90.00	84.27	5.73	6.37		
13	Lower	16	δ_1	74.00	75.59	1.59	2.15	Xin Zhuang Zi	(Wang, 2016)
14			δ_2	86.00	85.50	0.50	0.58		
15	Upper	9	δ_3	75.00	74.50	0.50	0.66	Sheng Yuan	(Chen CX, 2017)
16			δ_4	75.00	75.76	0.76	1.01		
17	Lower	4	δ_1	78.00	77.10	0.90	1.16	Ding Ji	(Xu QY, 2016)
18			δ_2	82.00	80.88	1.12	1.36		
19	Lower	16	δ_1	74.80	75.59	0.79	1.06	Xin Ji	(JJ, 2015)
20			δ_2	89.20	85.50	3.70	4.14		
21	Lower	7	δ_1	77.00	76.80	0.20	0.25	Pan Yi	(Wu Q, 2015)
22			δ_2	83.00	81.87	1.13	1.36		
23	Upper	19	δ_3	75.00	75.41	0.41	0.55	Yi Zhong	(Yang JW, 2015)

24			δ_4	75.00	73.87	1.13	1.50		
25	Upper	20	δ_3	75.00	75.56	0.56	0.74	Zi Jiang	(Chen Y, 2014)
26			δ_4	75.00	73.63	1.37	1.83		
27	Lower	5	δ_1	77.00	76.91	0.09	0.12	Gu Qiao	(Chen YK, 2012)
28			δ_2	82.00	81.19	0.81	0.99		
29	Upper	10	δ_3	75.00	74.53	0.47	0.62	Qi Nan	(YH, 2010)
30			δ_4	75.00	75.65	0.65	0.87		
31	Lower	8	δ_1	77.00	76.81	0.19	0.25	Pan San	(Gao S, 2003)
32			δ_2	84.50	82.25	2.25	2.67		

Table 5 also shows the maximum value, minimum value and mean of the absolute error for δ_m are of 5.73°, 0.09° and 1.41°, and the maximum value, minimum value and mean of the relative error are 6.55%, 0.12% and 0.73%, respectively. Fig.11 provides a comparison bar between the field measurements and the predicted values of δ_m, according to the data in Table 5.

Table 5 and Fig.11 show the predicted values are mostly consistent with the field measurements, which also verified the validity of the equaitons for δ_1, δ_2, δ_3 and δ_4.

3.4.3. Implication

The above analysis demonstrate that these equations can be computationally solved to calculated pressure relief angles for any given seam dips and have satisfactory accuracy, which can provide convenience for estimating the pressure relief angles along inclination as a kind of supplement and improvement for Detailed Rules on Prevention of Coal and Gas Outburst.

It should also be acknowledged that the pressure relief angles along inclination for protective seam mining are related to multiple geological and other factors besides coal seam dip angle. Further work needs be conducted to investigate the impact of geological and mining conditions on the pressure relief angles and develop a model with multi-factor parameters that are more appropriate for predicting the pressure relief angles in protective coal seam mining. It is more reliable to determine the pressure relief angles by field measurement because of the variation in geological conditions at different coalmines.

Nevertheless, when the field-testing method is adopted, a fixed number of testing boreholes must be drilled for measurement of the outburst prediction parameters (gas content or gas pressure), to determinate the pressure relief angles along inclination as shown in Fig.12 (Undergroundcoal, 2020; Wang et al., 2017a). Before field drilling,

it would be useful to estimate the pressure relief angles by the proposed functions, as the predicted data can be used as reference for borehole designs to improve the accuracy of borehole positioning and reduce the complexity of drilling and testing engineering.

4. Conclusions

Traditionally, pressure relief angles along seam inclination can be determined by discontinuous discrete data sets. However, it is difficult to infer its value for seam dips fall between the discrete datasets. Based on polynomial curve fitting method, mathematical equations for pressure relief angle and seam dip are derived to solve this problem.

The polynomial equations for δ_1, δ_2, δ_3 and δ_4 when the orders are selected as 7, 6, 4 and 5 respectively are recommended as the most suitable prediction functions for the pressure relief angles along inclination on protective seam mining.

These equations can be computationally solved to calculated pressure relief angles for any given seam dips, which have satisfied precision requirements and are convenient to use. The calculated results can provide a theoretical reference for the design and evaluation of protection zones in protective seam mining for eliminating coal and gas outburst risk. The equations are suggested as supplement and improvement for Detailed Rules on Prevention of Coal and Gas Outburst.

Declarations

Acknowledgements

This work was supported by the National Science and Technology Major Project of China (Nos. 2016ZX05067006-002; 2017ZX05064002).

Declaration of competing interests

The authors declare that they have no competing interests.

Authors' contributions

Zhen Zhang: Methodology, Data Curation, Data analysis, Writing-Original Draft

Gaofeng Liu: Conceptualization, Methodology, Data Curation, Writing-Original Draft, Writing-Review & Editing, Funding acquisition, Supervision

Ting Ren: Methodology, Formal analysis Writing-Review & Editing

Patrick Booth: Methodology, Formal analysis, Writing-Review & Editing

Runsheng Lv: Methodology, Data Curation, Formal analysis, Supervision

Jia Lin: Methodology, Data Curation, Formal analysis, Writing-Review & Editing

References

Aguado, M.B.D., Nicieza, C.G., 2007. Control and prevention of gas outbursts in coal mines, Riosa–Olloniego coalfield, Spain. International Journal of Coal Geology 69, 253-266.

Black, D.J., 2019. Review of coal and gas outburst in Australian underground coal mines. International Journal of Mining Science and Technology 29, 815-824.

Boyd, J.P., 2010. Six strategies for defeating the Runge Phenomenon in Gaussian radial basis functions on a finite interval. Computers & Mathematics with Applications 60, 3108-3122.

Cao, Z., He, X., Wang, E., Kong, B., 2018. Protection scope and gas extraction of the low-protective layer in a thin coal seam: lessons from the DaHe coalfield, China. Geosciences Journal 22, 487-499.

Chen CX, S.J., Li WB, 2017. Investigation on regional outburst prevention effect with mining of upper protective seam extraction. China Coal 47, 110-112.

Chen, X., Li, L., Wang, L., 2019a. The mechanical effect of typical dynamic disaster evolution and occurrence in coal mines. Energy Sources, Part A: Recovery, Utilization, and Environmental Effects, 1-12.

Chen, X., Li, L., Wang, L., Qi, L., 2019b. The current situation and prevention and control countermeasures for typical dynamic disasters in kilometer-deep mines in China. Safety science 115, 229-236.

Chen Y, Y.H., 2014. Study of Stress Displacement and Mining Influence on Protected Seam in Extraction of Gently-inclined Contiguous Upper Protective Seam. Mining Safety & Environmental Protection 41, 1-3+8.

Chen YK, Y.D., Jiang XL, 2012. Stereo Methane Drainage Technology of Protective Coal-seam Mining Face in Guqiao Colliery. Coal Mining Technology 17, 84-87.

Cheng, Y., 2010. Mine gas hazard control theory and engineering application. China university of mining and technology press, Xuzhou.

Deboeverie, F., Teelen, K., Veelaert, P., Philips, W., 2010. Adaptive constructive polynomial fitting, International Conference on Advanced Concepts for Intelligent Vision Systems. Springer, pp. 173-184.

Feng, Y., Wang, S.J., Sha, Y., Ding, Q.Z., Yuan, J.H., Guo, X.P., 2018. Coal power overcapacity in China: Province-Level estimates and policy implications. Resources Conservation and Recycling 137, 89-100.

Fornberg, B., Zuev, J., 2007. The Runge phenomenon and spatially variable shape parameters in RBF interpolation. Computers & Mathematics with Applications 54, 379-398.

Gao S, S.B., 2003. Practice of mining technology of lower protective layer under long distance in Pansan mine. Safety in Coal Mines Safety in Coal Mines 23-25.

Guest, P.G., 2012. Numerical methods of curve fitting. Cambridge University Press.

Han, J., Zhang, H.W., Li, S., Song, W.H., 2012. The characteristic of in situ stress in outburst area of China. Safety science 50, 878-884.

He, X., Chen, W., Nie, B., Zhang, M., 2010. Classification technique for danger classes of coal and gas outburst in deep coal mines. Safety science 48, 173-178.

Hedlund, F.H., 2012. The extreme carbon dioxide outburst at the Menzengraben potash mine 7 July 1953. Safety science 50, 537-553.

Jia, T., Zhang, Z., Tang, C., Zhang, Y., 2013. Numerical simulation of stress-relief effects of protective layer extraction. Archives of Mining Sciences 58.

Jin, K., Cheng, Y.P., Wang, W., Liu, H.B., Liu, Z.D., Zhang, H., 2016. Evaluation of the remote lower protective seam mining for coal mine gas control: A typical case study from the Zhuxianzhuang Coal Mine, Huaibei Coalfield, China. Journal of Natural Gas Science and Engineering 33, 44-55.

JJ, C., 2015. Test of Far-distance Lower Protective Coal-seam Mining in Xinji 1st Mine. Coal Mining Technology 20, 26-29.

Karakus, D., 2013. FINDING THE BEST-FIT POLYNOMIAL APPROXIMATION IN EVALUATING DRILL DATA: THE APPLICATION OF A GENERALIZED INVERSE MATRIX/POSZUKIWANIE NAJLEPSZEJ ZGODNOŚCI W PRZYBLIŻENIU WIELOMIANOWYM WYKORZYSTANEJ DO OCENY DANYCH Z ODWIERTÓW–ZASTOSOWANIE UOGÓLNIONEJ MACIERZY ODWROTNEJ. Archives of Mining Sciences 58, 1289-1300.

Li, W., Cheng, Y.-p., Guo, P.-k., An, F.-h., Chen, M.-y., 2014. The evolution of permeability and gas composition during remote protective longwall mining and stress-relief gas drainage: a case study of the underground Haishiwan Coal Mine. Geosciences Journal 18, 427-437.

Liang, Y., 2018. Strategies of High Efficiency Recovery and Energy Saving for Coal Resources in China. Journal of China University of Mining & Technology (Social Sciences), 1.

Liu, A., Tu, S., Wang, F., Yuan, Y., Zhang, C., Zhang, Y., 2013. Numerical simulation of pressure relief rule of upper and lower protected coal-seam in thin-protective-seam mining. Disaster Advances 6, 16-25.

LIU, C.-a., YANG, J.-w., 2013. Seam Inclination Affected to Evolution Law of Mining Cracks. Coal Science and Technology 3.

Liu, H., Cheng, Y., 2015. The elimination of coal and gas outburst disasters by long distance lower protective seam mining combined with stress-relief gas extraction in the Huaibei coal mine area. Journal of Natural Gas Science and Engineering 27, 346-353.

Liu, Z., Yang, H., Cheng, W., Xin, L., Ni, G., 2017. Stress distribution characteristic analysis and control of coal and gas outburst disaster in a pressure-relief boundary area in protective layer mining. Arabian Journal of Geosciences 10, 358.

O'Hagan, A., 1978. Curve fitting and optimal design for prediction. Journal of the Royal Statistical Society: Series B (Methodological) 40, 1-24.

Rong H, Z.H., Zhu ZJ, et al, 2019. Optimization scheme in mining in hope to protect the ultra-thick suberect coal seams off the potential rock burst risks. Journal of Safety and Environment 19, 1182-1191.

S, G., 2019. Research on Protective Range by Protective Seam Exploitation in Xieqiao Mine. Coal Technology 5, 46-49.

Safety, C.s.S.A.o.W., 2019. Detailed Rules on Prevention of Coal and Gas Outburst http://www.gov.cn/xinwen/2019-08/21/content_5423024.htm.

Saleh, J.H., Cummings, A.M., 2011. Safety in the mining industry and the unfinished legacy of mining accidents: Safety levers and defense-in-depth for addressing mining hazards. Safety science 49, 764-777.

Seifert, E., 2014. OriginPro 9.1: Scientific Data Analysis and Graphing Software– Software Review. ACS Publications.

Shang, Z., Wang, H., Cheng, Y., Li, B., Dong, J., Liu, Q., 2019. Optimal selection of coal seam pressure-relief gas extraction technologies: a typical case of the Panyi Coal Mine, Huainan coalfield, China. Energy Sources, Part A: Recovery, Utilization, and Environmental Effects, 1-21.

Skoczylas, N., Dutka, B., Sobczyk, J., 2014. Mechanical and gaseous properties of coal briquettes in terms of outburst risk. Fuel 134, 45-52.

Sobczyk, J., 2014. A comparison of the influence of adsorbed gases on gas stresses leading to coal and gas outburst. Fuel 115, 288-294.

State administration of market ragulation, S.a., 2019. Methods for test,monitoring and prevention of rock burst—Part 12: Prevention method of protective seam mining, https://www.spc.org.cn/basicsearch.

Tibshirani, R.J., 2014. Adaptive piecewise polynomial estimation via trend filtering. The Annals of Statistics 42, 285-323.

Tu, Q., Cheng, Y., 2019. Stress evolution and coal seam deformation through the mining of a remote upper protective layer. Energy Sources, Part A: Recovery, Utilization, and Environmental Effects 41, 338-348.

Undergroundcoal, 2020. Gas Content: direct method, http://www.undergroundcoal.com.au/outburst/direct.aspx.

Wang, B., Wu, C., Kang, L., Reniers, G., Huang, L., 2018. Work safety in China's Thirteenth Five-Year plan period (2016–2020): Current status, new challenges and future tasks. Safety science 104, 164-178.

Wang, B.W., P, 2016. Research on Gas Relief Drainage Technology of Lower Protective Layer Mining. Coal Technology 35, 203-204.

Wang, C., Yang, S., Jiang, C., Yang, D., Zhang, C., Li, X., Chen, Y., Tang, J., 2017a. A method of rapid determination of gas pressure in a coal seam based on the advantages of gas spherical flow field. Journal of Natural Gas Science and Engineering 45, 502-510.

Wang, G., Wu, M.M., Wang, R., Xu, H., Song, X., 2017b. Height of the mining-induced fractured zone above a coal face. Engineering Geology 216, 140-152.

Wang, H., Cheng, Y., Yuan, L., 2013a. Gas outburst disasters and the mining technology of key protective seam in coal seam group in the Huainan coalfield. Natural Hazards 67, 763-782.

Wang, H., Wang, Z., Fan, X., Liu, N., Liu, J., 2010. Numerical simulation for protection scope of steep inclined upper-protective layer of pitching oblique mining. Disaster Advances 3, 546-550.

Wang, L., Cheng, Y.-P., Liu, H.-Y., 2014. An analysis of fatal gas accidents in Chinese coal mines. Safety science 62, 107-113.

Wang, L., Cheng, Y.-p., Wang, L., Guo, P.-k., Li, W., 2012. Safety line method for the prediction of deep coal-seam gas pressure and its application in coal mines. Safety science 50, 523-529.

Wang, L., Cheng, Y.P., Xu, C., An, F.H., Jin, K., Zhang, X.L., 2013b. The controlling effect of thick-hard igneous rock on pressure relief gas drainage and dynamic disasters in outburst coal seams. Natural Hazards 66, 1221-1241.

Wu, L., Jiang, Z., Cheng, W., Zuo, X., Lv, D., Yao, Y., 2011. Major accident analysis and prevention of coal mines in China from the year of 1949 to 2009. Mining Science and Technology (China) 21, 693-699.

Wu Q, S.B., Mu ZM, et al, 2015. Rationality Study of Protection Scope of Underside Protective Layer Mining in East Region of Panyi Mine. Safety in Coal Mines 46, 12-15.

Xie, H., Gao, F., Ju, Y., Gao, M.-z., Zhang, R., Gao, Y.-n., Liu, J.-f., Xie, L.-z., 2015. Quantitative definition and investigation of deep mining. Journal of China Coal Society 40, 1-10.

Xie, H., Qian, M., Peng, S., Hu, X., Cheng, Y., Zhou, H., 2011. Sustainable capacity of coal mining and its strategic plan. Engineering Sciences 13, 44-50.

Xie, J.-L., Xu, J.-L., 2017. Effect of key stratum on the mining abutment pressure of a coal seam. Geosciences Journal 21, 267-276.

Xiong, Z.T., GM; Yuan, GY, 2014. Pressure relief boundary of protected seam mining with subhorizontal long-distance. Journal of Xi'an University of Science and Technology 34, 147-151.

Xu, L., Lu, K., Pan, Y., Qin, Z., 2019. Study on rock burst characteristics of coal mine roadway in China. Energy Sources, Part A: Recovery, Utilization, and Environmental Effects, 1-20.

Xu QY, Y.M., Qiao YD, et al, 2016. Study on pressure-relief protection scope of lower protective seam mining. Coal Engineering 48, 79-82.

Xue, S., Yuan, L., 2017. The use of coal cuttings from underground boreholes to determine gas content of coal with direct desorption method. International Journal of Coal Geology 174, 1-7.

Yang JW, H.W., Chen JY, 2015. Closed Distance Coal Seam Group in Application of Upper Protective Layer Mining in Yizhong Coal Mine. Coal Technology 34, 21-23.

Yang, W., Lin, B.-q., Qu, Y.-a., Zhao, S., Zhai, C., Jia, L.-l., Zhao, W.-q., 2011. Mechanism of strata deformation under protective seam and its application for relieved methane control. International Journal of Coal Geology 85, 300-306.

YH, L., 2010. Pressure relief gas drainage technology for mining upper protective layer in Qinan mine. Safety in Coal Mines 41, 33-35.

Yin, G., Li, M., Wang, J., Xu, J., Li, W., 2015. Mechanical behavior and permeability evolution of gas infiltrated coals during protective layer mining. International Journal of Rock Mechanics and Mining Sciences 80, 292-301.

Yin, W., Fu, G., Yang, C., Jiang, Z., Zhu, K., Gao, Y., 2017. Fatal gas explosion accidents on Chinese coal mines and the characteristics of unsafe behaviors: 2000–2014. Safety science 92, 173-179.

Yongqi, X., 2004. Coal Mining. China University of mining and Technology Press, Xuzhou.

Yu, B., 1986. Understanding and practice of mining protective seam. Coal Industry Press, Beijing.

Yuan, L., 2016. Control of coal and gas outbursts in Huainan mines in China: A review. Journal of Rock Mechanics and Geotechnical Engineering 8, 559-567.

Yuan, L., Xue, S., 2014. Defining outburst-free zones in protective mining with seam gas content-method and application. Journal of China Coal Society 39, 1786-1791.

Zhang, B., Guan, S.H., Wu, X.F., Zhao, X.L., 2018. Tracing natural resource uses via China's supply chains. Journal of Cleaner Production 196, 880-888.

Zhang, C., Tu, S., Zhang, L., Wang, F., Bai, Q., Tu, H., 2016. The numerical simulation of permeability rules in protective seam mining. International Journal of Oil, Gas and Coal Technology 13, 243-259.

Zhang, H., Cheng, Y., Yuan, L., Wang, L., Jiang, J., Li, G., 2019. Gas extraction challenge and the application of hydraulic cavity technology in the Shijiazhuang coalmine, Qinshui basin. Energy Sources, Part A: Recovery, Utilization, and Environmental Effects, 1-23.

Zhang, R., Cheng, Y., Yuan, L., 2020. Study on the stress relief and permeability increase in a special low-permeability thick coal seam to stimulate gas drainage. Energy Sources, Part A: Recovery, Utilization, and Environmental Effects 42, 1001-1013.

Zhao Z, L.Y., Zhou Y, 2016. Application of Preventive Layer Mining Technique in Outburst Mine with Large Mining Depth. Safety in Coal Mines 47, 135-138.

Figures

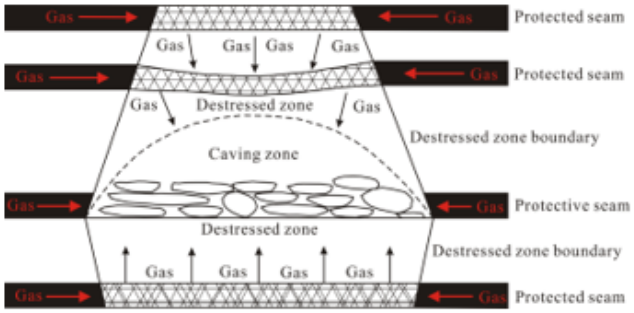

Figure 1

Diagram of reducing outburst on protective seam mining

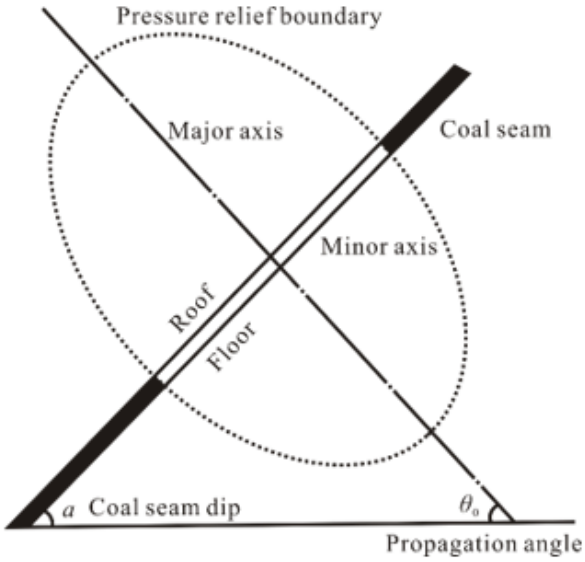

Figure 2

Diagram of pressure relief zone distribution along inclination of coal seam(Yu, 1986)

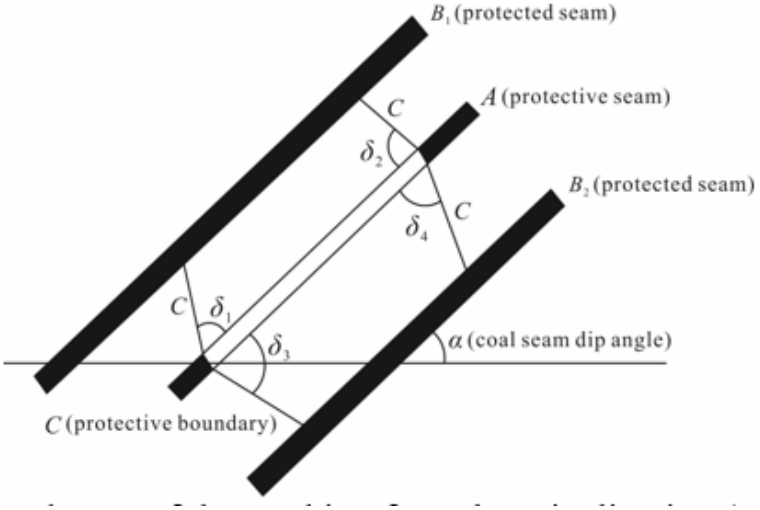

Figure 3

Protected zone of the working face along inclination (Safety, 2019)

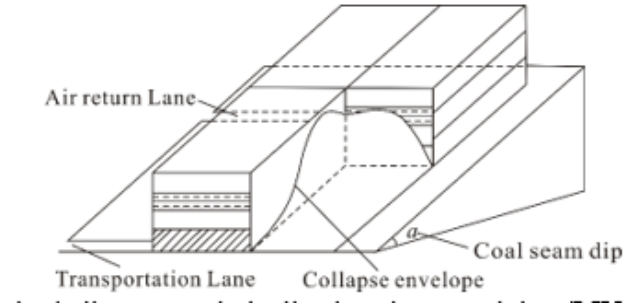

Figure 4

Asymmetric shell structure in inclined coal seam mining (LIU and YANG, 2013)

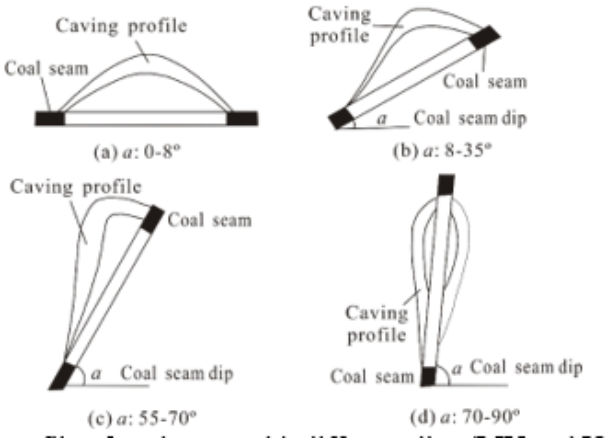

Figure 5

Caving profile of coal seam with different dips (LIU and YANG, 2013)

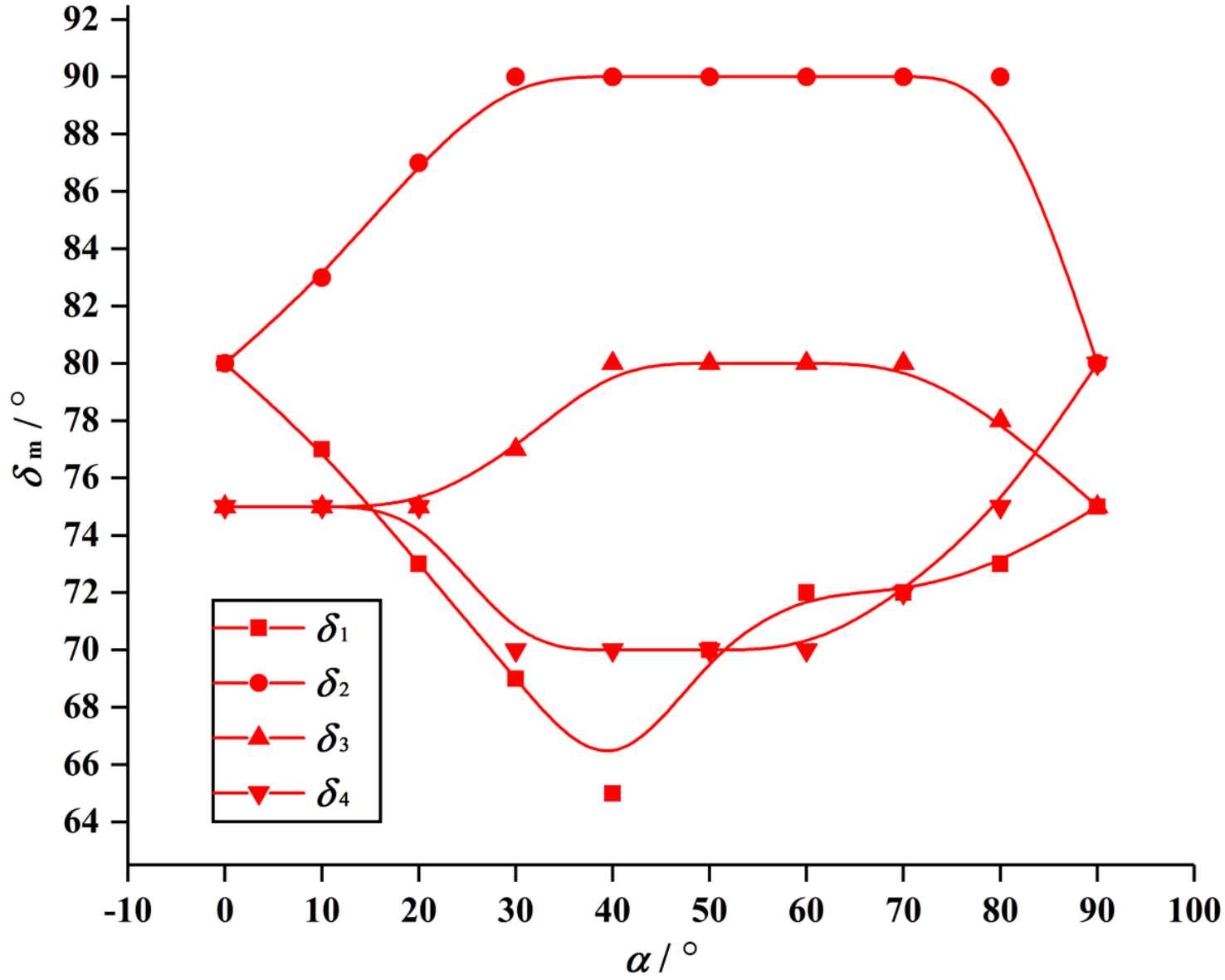

Figure 6

Curve of pressure relief angles δm with coal seam dip a

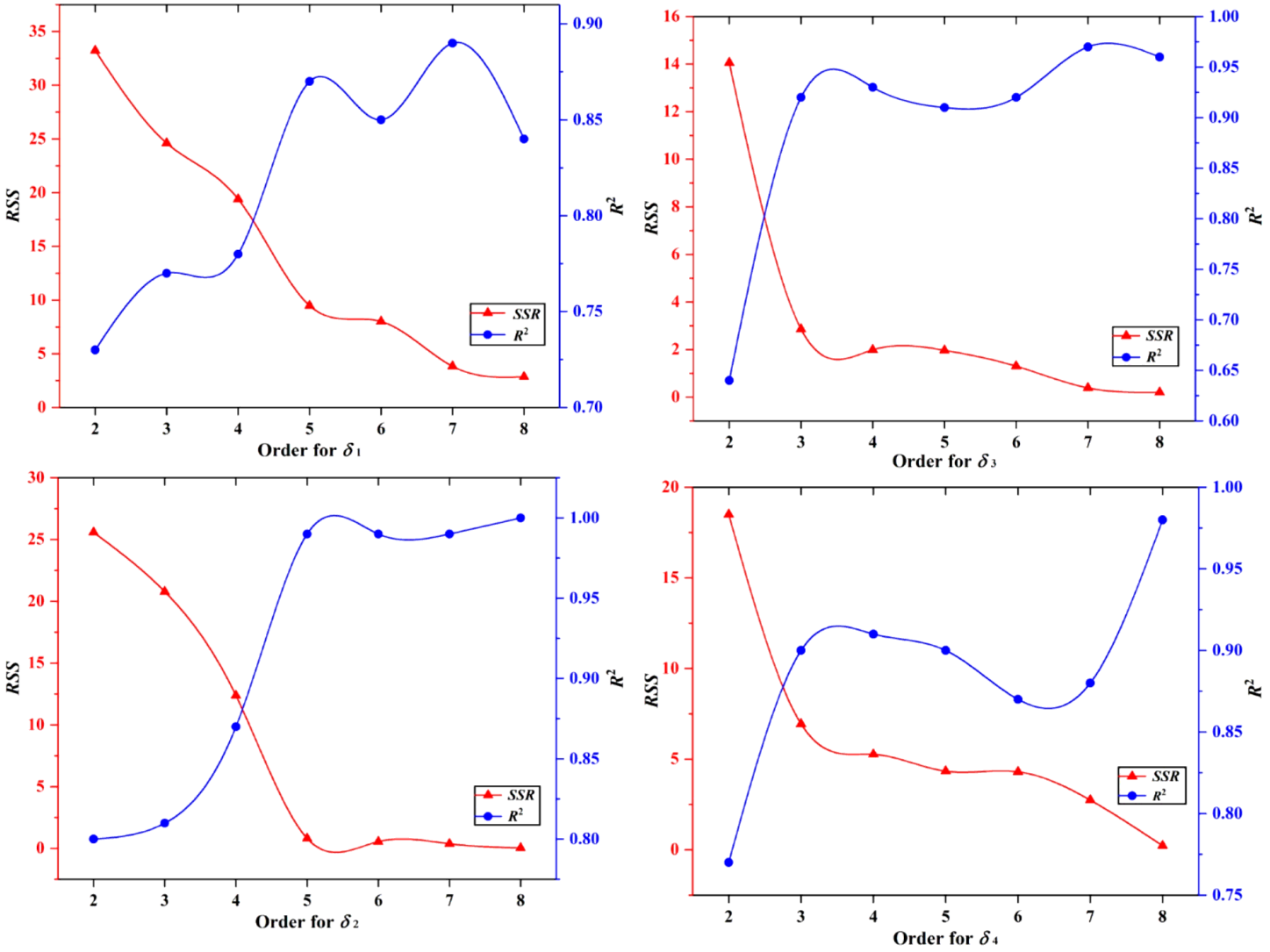

Figure 7

Curves of RSS and R2 with the polynomial order for δm

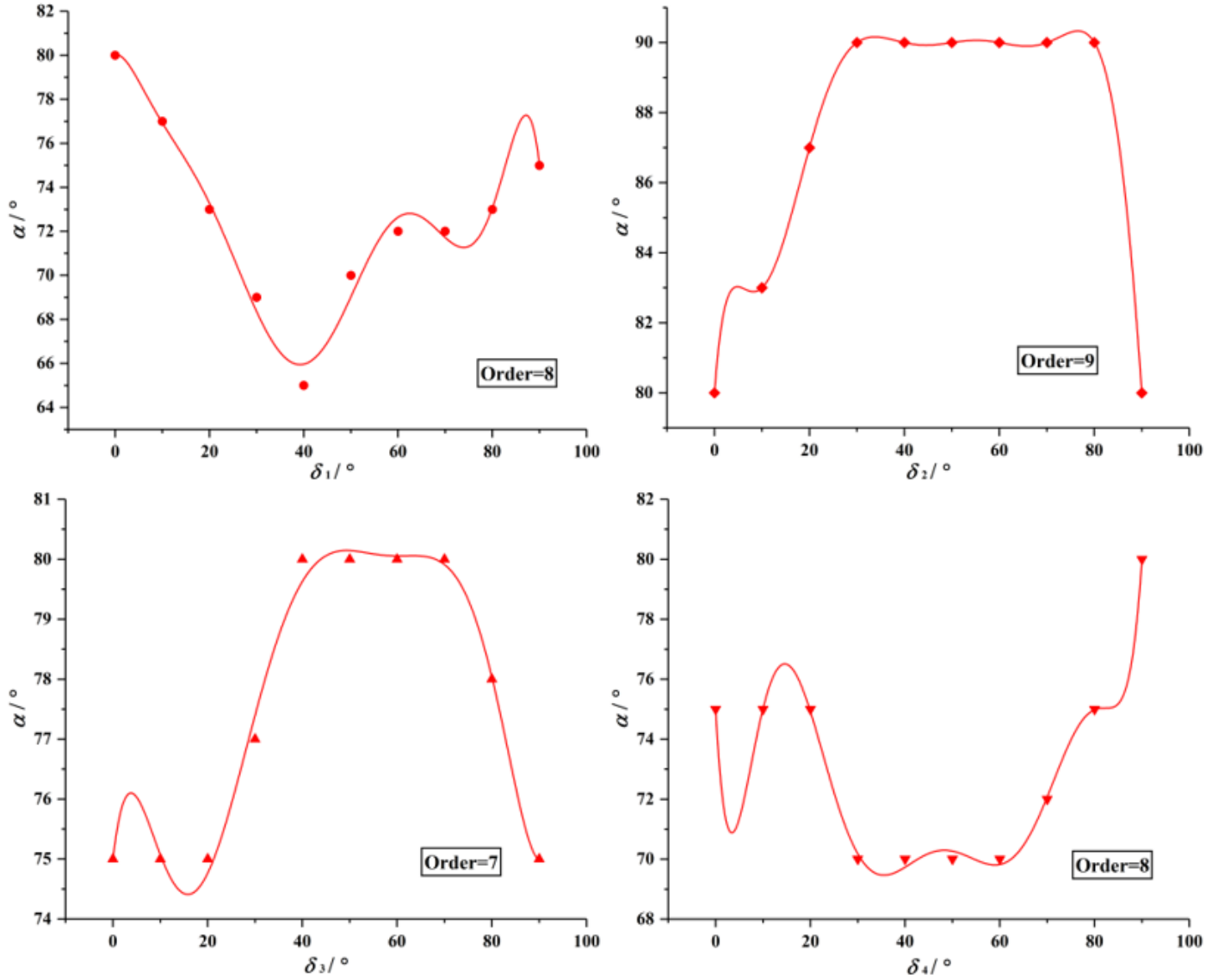

Figure 8

Lowest orders resulting in Runge phenomenon for δm

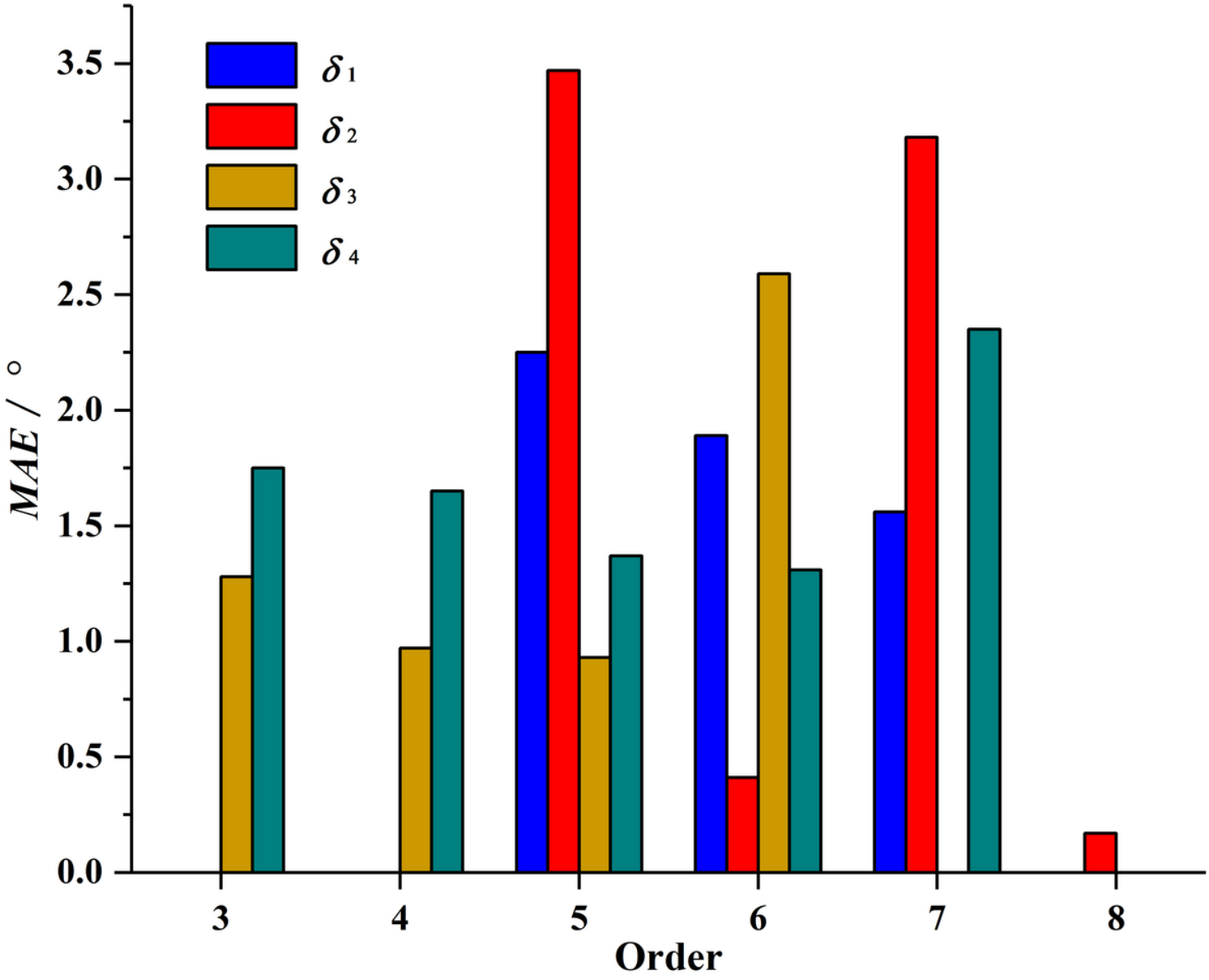

Figure 9

Comparison of MAE with model order for δm

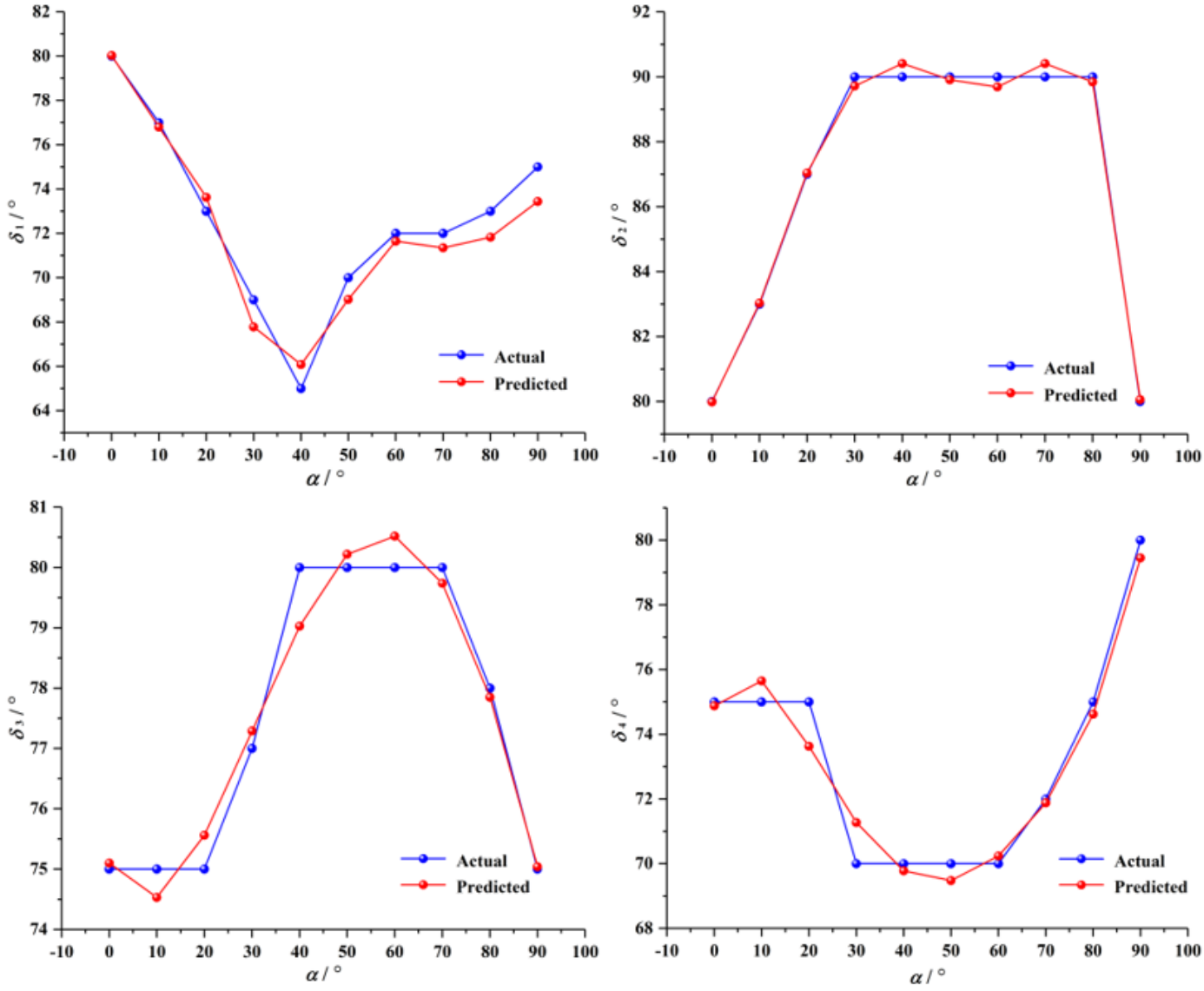

Figure 10

Comparison curves between the actual value and the predicted value

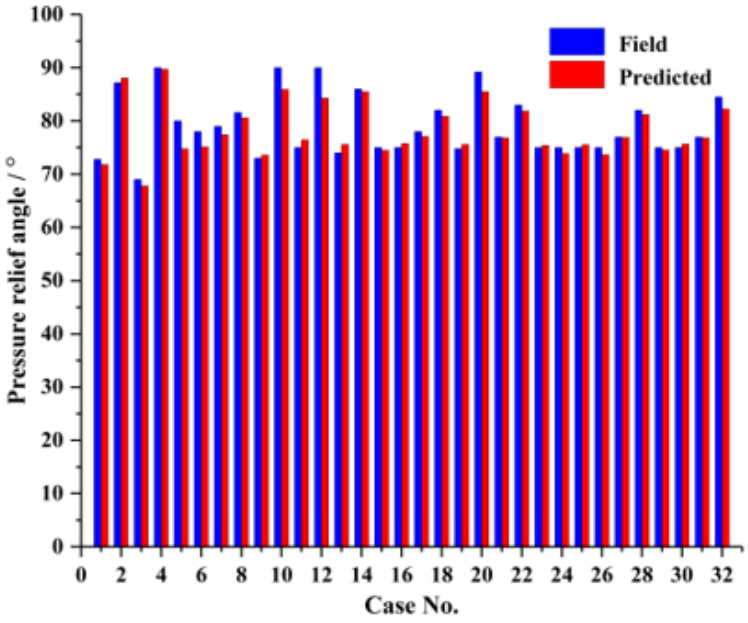

Figure 11

Comparison chart of the field-testing value and the predicted value

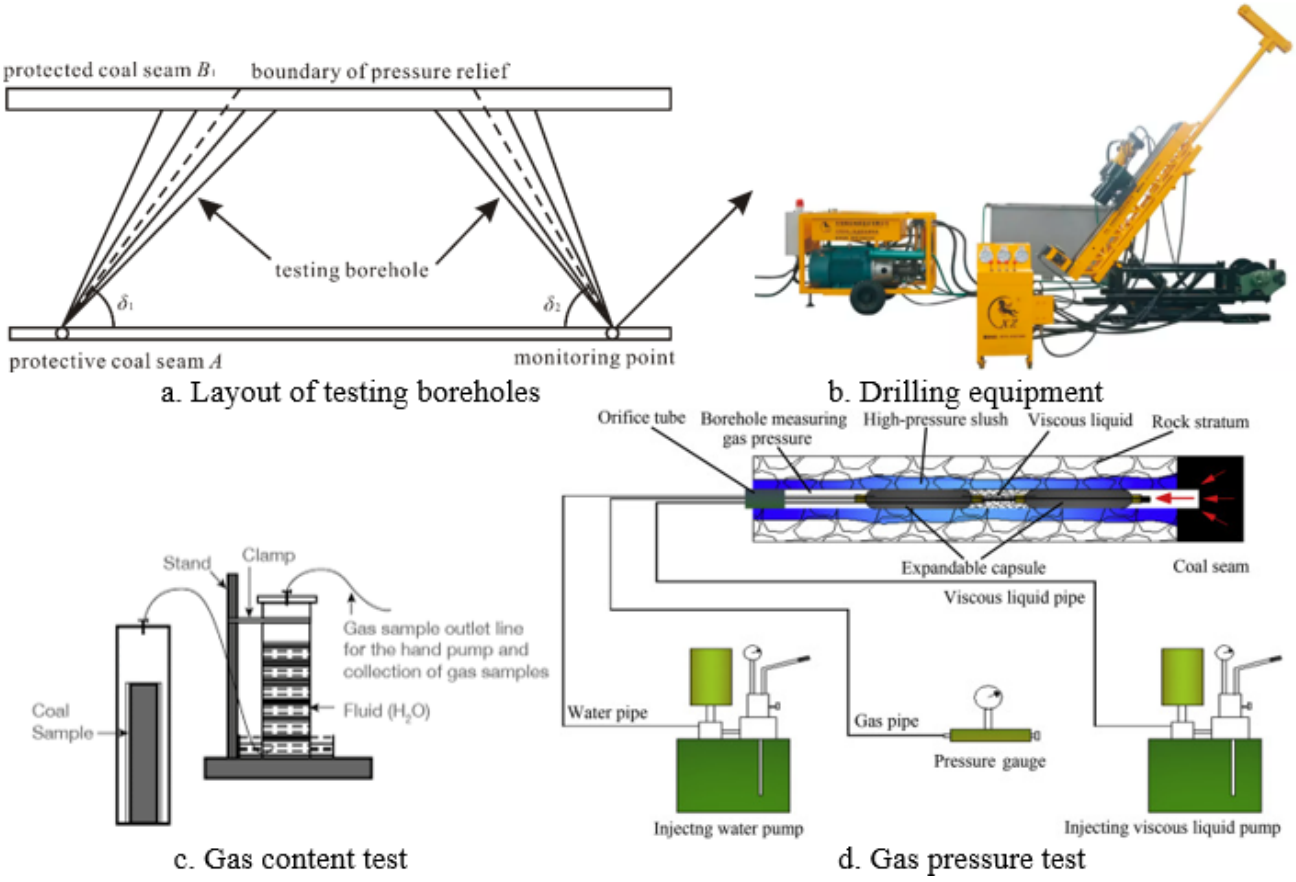

Figure 12

Diagram of field-testing to determinate the pressure relief angles